ACS OMEGA

Open Access

This article is licensed under CC-BY-NC-ND 4.0

http://pubs.acs.org/journal/acsodf

Article

Pyrolysis Characteristics and Determination of Kinetic and Thermodynamic Parameters of Raw and Torrefied Chinese Fir

Yogesh Patil, Xiaoke Ku,* and Vikul Vasudev

Cite This: *ACS Omega* 2023, 8, 34938−34947

Read Online

ACCESS | Metrics & More | Article Recommendations

ABSTRACT: Torrefaction influences the structural and physicochemical properties of biomass, thus further altering its thermal degradation behavior. In this study, the pyrolysis characteristics, reaction kinetics, and thermodynamic parameters of raw and torrefied Chinese fir (CF) were investigated. The torrefaction was conducted at 220 °C (mild) and 280 °C (severe), the pyrolysis was performed from ambient temperature to 600 °C, and four different heating rates (i.e., 5, 15, 25, and 35 °C/min) were adopted. The activation energy for pyrolysis was estimated by adopting three isoconversional methods. The master-plot method was employed to analyze the reaction mechanism. Furthermore, thermodynamic parameters, i.e., the enthalpy change (ΔH), Gibbs free energy change (ΔG), and entropy change (ΔS), were calculated. The average activation energy increased with the torrefaction temperature, whose values estimated by using different methods ranged from 88.57 to 97.70, from 121.04 to 126.35, and from 167.51 to 179.74 kJ/mol for raw, mildly, and severely torrefied CF samples, respectively. A compensation effect between the activation energy and pre-exponential factor was observed for all samples. The degradation process was characterized as endothermic, involving the formation of activated complexes and requiring extra energy for torrefied samples.

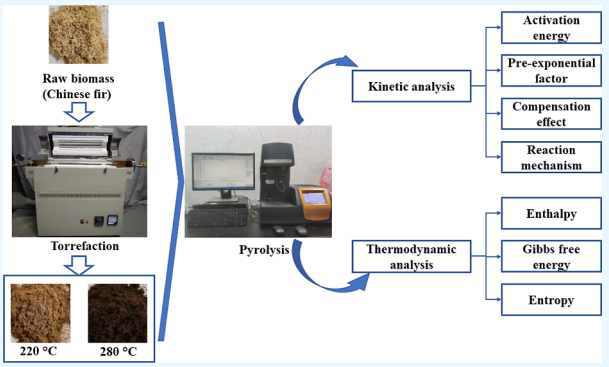

1. INTRODUCTION

Population explosions and increased energy consumption have raised a range of environmental concerns. Thus, exploring clean alternative energy sources has gained much interest in recent years. Biomass is considered a carbon-neutral energy source because the carbon released during its energy utilization is almost offset by the carbon absorbed during its growth. Consequently, its wide use can help reduce pollution emissions (e.g., CO_2 and SO_x).[1−3] Among different biomass types, lignocellulosic biomass, generally regarded as woody biomass, contains a large quantity of carbon and possesses the potential to generate useful energy products in solid, liquid, and gaseous forms. It mainly consists of three major components, i.e., hemicellulose, cellulose, and lignin. Hemicellulose is a large family of polysaccharides and normally undergoes significant thermal degradation in the temperature range of 200−350 °C.[4] Cellulose is a glucose polymer which experiences the initial and major degradations in the temperature ranges of around 200−250 and 300−400 °C, respectively. Moreover, lignin is an aromatic polymer and decomposes over a wide temperature range.[5,6]

The thermochemical conversion of biomass to fuel depends on many factors, such as biomass characteristics and process parameters. Also, the conversion efficiency might decrease due to some inherent shortcomings of raw biomass, such as high moisture content and hygroscopicity and low energy density. Over the years, several pretreatment processes have been proposed, which can alter the biomass properties and make it more suitable for conversion. Torrefaction is one such pretreatment process that has been utilized to enhance the fuel properties of biomass.[7,8] During torrefaction, raw biomass is generally heated in the range of 200−350 °C for a certain time period and undergoes physical and chemical changes, e.g., the decomposition of hemicellulose and depolymerization or partial degradation of cellulose and lignin.[9−11] Consequently, the moisture and some solid contents are lost, and the solid products can be used as fuel, soil amendment, carbon sequestration, and water filtration.[12] Doddapaneni et al. (2016)[13] analyzed the impact of torrefaction on the pyrolysis of Eucalyptus clones. They revealed that the char content after pyrolysis increased with the torrefaction temperature. Moreover, an enhancement in the thermal stability of the torrefied biomass was also observed. Cao et al. (2021)[14] investigated the effect of

Received: June 18, 2023
Accepted: September 1, 2023
Published: September 15, 2023

© 2023 The Authors. Published by American Chemical Society

Table 1. Expressions of Various Solid-State Reaction Models and Their $g(\alpha)$ and $f(\alpha)$

notation	mechanism	integral form, $g(\alpha)$	differential form, $f(\alpha)$
		Nucleation Models	
P3	power law	$\alpha^{(1/3)}$	$3\alpha^{(2/3)}$
P4	power law	$\alpha^{(1/4)}$	$4\alpha^{(3/4)}$
A3	Avrami-Erofeev	$[-\ln(1-\alpha)]^{(1/3)}$	$3(1-\alpha)[-\ln(1-\alpha)]^{(2/3)}$
		Reaction Order Models	
F1	$n = 1$	$-\ln(1-\alpha)$	$(1-\alpha)$
		Geometrical Contraction Models	
R1	one dimension	α	1
R2	contracting cylinder	$1-(1-\alpha)^{(1/2)}$	$2(1-\alpha)^{(1/2)}$
		Diffusion Models	
D2	two-dimensional diffusion	$(1-\alpha)\ln(1-\alpha)+\alpha$	$[-\ln(1-\alpha)]^{-1}$
D3	three-dimensional diffusion (Jander equation)	$(1-(1-\alpha)^{1/3})^2$	$[3(1-\alpha)^{(2/3)}]/[2(1-(1-\alpha)^{(1/3)})]$
D4	three-dimensional diffusion (Ginstling equation)	$1-(2/3)\alpha-(1-\alpha)^{(2/3)}$	$3/[2((1-\alpha)^{(-1/3)}-1)]$

torrefaction temperature on cellulose pyrolysis characteristics. They reported that the highest torrefaction temperature (i.e., 290 °C) yielded the maximum oxygen removal, highest carbonization, and higher heating values (HHVs). They further found that torrefaction pretreatment not only influenced the physical and chemical properties of biomass but also altered the product yield during pyrolysis.

To convert biomass into energy, various thermochemical processes have been developed. Of these, pyrolysis can convert biomass into various energy products, e.g., bio-char, bio-oil, and biogas.[15] Patidar et al. (2022)[16] studied the pyrolysis of different biomasses and analyzed their potential applications for bioenergy production. During pyrolysis, the kinetic and thermodynamic analyses are crucial for comprehending the thermal degradation behavior as well as process design and optimization.[17,18] Singh et al. (2021)[19] gave some insights into the kinetic and thermodynamic behaviors of the pyrolysis of rice straw. Ahmad et al. (2021)[20] evaluated the kinetic and thermodynamic parameters of maple leaf waste using isoconversional methods. They found that the values of Gibbs free energy change ranged from 216 to 325 kJ/mol. Other works were also dedicated to a better understanding of the biomass pyrolysis process.[21,22] However, few studies focus on the pyrolysis behaviors, reaction mechanisms, and thermodynamic analysis of torrefied biomass.[23]

Therefore, in this work, a comprehensive investigation of physicochemical properties and pyrolysis characteristics of raw and torrefied Chinese fir (CF) was performed. Note that CF is a coniferous evergreen timber tree of the cypress family and is also an important commercial timber species in China.[24] To explore the effect of torrefaction on pyrolysis, two distinct torrefaction temperatures (i.e., 220 and 280 °C) and four different pyrolysis heating rates (i.e., 5, 15, 25, and 35 °C/min) were selected. The activation energy for pyrolysis was estimated by adopting three different isoconversional methods, i.e., the Starink, Boswell, and Friedman methods. The master-plot method was employed to analyze the reaction mechanism followed by raw and torrefied biomass samples. In addition, three thermodynamic parameters, i.e., the enthalpy change (ΔH), Gibbs free energy change (ΔG), and entropy change (ΔS), were also calculated. All these results are beneficial to deeply understanding the pyrolysis process of raw and torrefied CF.

2. MATERIALS AND METHODS

2.1. Sample. To conduct torrefaction and pyrolysis experiments, CF was used as the biomass fuel. It was obtained from Tianxu Energy, located in Guangzhou, China. The biomass was dried, ground, sieved, and finally had an average particle size of around 98 μm. Then, the powder samples were stored in an airtight container to avoid moisture absorption. The ultimate analyses were conducted using CHN-2000 and 5E-IRSII sulfate analyzers. The proximate analyses were carried out according to the experimental procedures of Qin and Thunman.[25] Moreover, the HHVs were estimated by using the empirical correlation proposed by Friedl et al. (2005).[26]

Table 2. Properties of Raw and Torrefied Biomass Samples

parameters	raw CF	CF220	CF280
	Proximate Analysis[a], wt (%)		
M[b]	8.36 ± 0.21	3.36 ± 0.21	1.97 ± 0.42
VM[c]	76.30 ± 0.75	51.58 ± 0.67	28.83 ± 0.85
FC[d,e]	14.42	42.01	64.89
ash	0.92 ± 0.01	3.05 ± 0.25	4.31 ± 0.24
	Ultimate Analysis[f], wt (%)		
C	52.38 ± 0.25	56.32 ± 0.10	63.25 ± 0.30
H	6.95 ± 0.07	6.29 ± 0.08	5.83 ± 0.03
N	0.33 ± 0.02	0.52 ± 0.03	0.57 ± 0.03
S	0.24 ± 0.03	0.17 ± 0.01	0.18 ± 0.09
O[e]	40.10	36.70	30.17
HHV (MJ/kg)	21.37 ± 0.15	22.97 ± 0.08	26.13 ± 0.14

[a]As-received basis. [b]M denotes moisture. [c]VM is volatile matter. [d]FC represents fixed carbon. [e]Calculated by difference. [f]Dry and ash-free basis.

2.2. Experimental Procedures. *2.2.1. Torrefaction.* For torrefaction, a horizontal quartz tube furnace (SG-GL1100K-100) manufactured by Zhuochi Instrument Co., Ltd. (Hangzhou, China) was used. To achieve an inert atmosphere inside the furnace, the nitrogen was purged continuously for 30 min prior to each experiment. Then, approximately 3 g of biomass sample was kept in a quartz boat and placed in the middle of the tube. The reactor temperature was first set to 30 °C, which was further increased to the torrefaction temperature (e.g., 220 or 280 °C) at a heating rate of 10 °C/min. After reaching the specified temperature, it was maintained for 40 min. The volatiles released during torrefaction were blown out of the

https://doi.org/10.1021/acsomega.3c04328
ACS Omega 2023, 8, 34938−34947

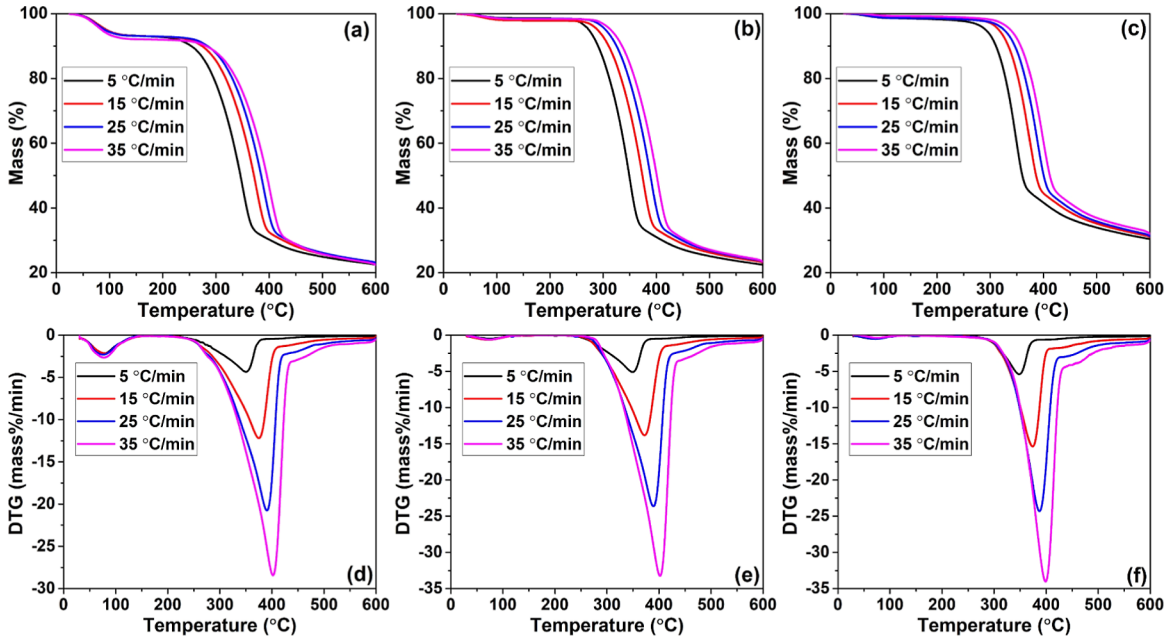

Figure 1. Thermogravimetric (TG) and differential thermogravimetric (DTG) curves for pyrolysis of (a,d) raw CF, (b,e) CF220, and (c,f) CF280 samples at different pyrolysis heating rates.

tube by nitrogen. Subsequently, the quartz boat was removed from the furnace and allowed to cool down to room temperature. Note that the quartz tube was cleaned before starting a new experiment. To differentiate torrefied samples, they were named with the first two letters representing the biomass type and the last three digits indicating the torrefaction temperature. For example, CF220 represents the sample of Chinese fir torrefied at 220 °C.

2.2.2. Pyrolysis. Pyrolysis experiments were performed in a thermogravimetric analyzer (TGA55, TA instruments). Specifically, approximately 10 mg of sample was placed in the furnace, and the temperature was first raised from room temperature to 150 °C at a heating rate of 20 °C/min. Then, to explore the effect of heating rate, the temperature is further raised from 150 to 600 °C by four different heating rates (i.e., 5, 15, 25, and 35 °C/min). Furthermore, to maintain an inert atmosphere during pyrolysis, nitrogen was purged with a flow rate of 40 mL/min.

2.3. Kinetic Parameters. Different biomass samples have different compositions and physical properties, resulting in distinct pyrolysis characteristics. To conduct pyrolysis kinetic analysis, three methods, i.e., the Starink, Boswell, and Friedman methods,[27−29] were employed to evaluate the activation energy E_α.

The pyrolytic degradation of biomass can be treated as a single-step reaction, and the conversion fraction α is defined as follows

$$\alpha = \frac{M_0 - M}{M_0 - M_f} \tag{1}$$

where M_0, M, and M_f are the initial, instantaneous, and final masses, respectively. Consequently, the reaction rate is expressed as[30,31]

$$\frac{d\alpha}{dt} = A\exp\left(\frac{-E_\alpha}{RT}\right)f(\alpha) \tag{2}$$

where t, T, A, R, and f are the time, temperature, pre-exponential factor, universal gas constant, and kinetic model, respectively. The integral form of eq 2 can be written as

$$g(\alpha) = \int_0^\alpha \frac{d\alpha}{f(\alpha)} = \frac{A}{\beta}\int_{T_0}^{T} \exp\left(\frac{-E_\alpha}{RT}\right)dT \tag{3}$$

where $\beta = dT/dt$ is the heating rate.

The equations for the Starink, Boswell, and Friedman methods are shown by eqs 4−6, respectively.[22,32,33]

$$\ln\left[\frac{\beta}{T^{1.92}}\right] = C - 1.0008\frac{E_\alpha}{RT} \tag{4}$$

$$\ln\left[\frac{\beta}{T}\right] = -\frac{E_\alpha}{RT} + C \tag{5}$$

$$\ln\left[\frac{d\alpha}{dt}\right] = \ln[Af(\alpha)] - \frac{E_\alpha}{RT} \tag{6}$$

For each method, plot the left-hand side of its equation versus $1/T$. As a result, E_α can be evaluated from the slope of the fitted line. Furthermore, A is calculated by using eq 7.[34,35]

$$A = \frac{\beta E_\alpha \exp\left(\frac{E_\alpha}{RT_m}\right)}{RT_m^{\,2}} \tag{7}$$

where T_m is the temperature at the peak of the major thermal degradation of the biomass sample. Note that β = 35 °C/min was selected to calculate A. Then, the compensation effect between E_α and A was also analyzed.

2.4. Determination of the Reaction Model. To understand the inherent reaction mechanism of biomass pyrolysis, the reaction model was determined using the master-plot method.[36] It was analyzed using the following equation[37]

https://doi.org/10.1021/acsomega.3c04328
ACS Omega 2023, 8, 34938−34947

Table 3. Temperatures and Mass Fractions at the Start, Peak, and End of the Major Thermal Degradation of Raw and Torrefied CF Samples

species	heating rate (°C/min)	T_a (°C)	T_m (°C)	T_c (°C)	M_a (%)	M_m (%)	M_c (%)
raw CF	5	195.97	350.38	385.41	92.77	46.09	31.53
	15	198.85	374.90	412.96	92.85	46.99	31.15
	25	212.90	390.47	420.45	92.84	45.40	31.37
	35	227.11	402.12	443.56	91.75	44.74	29.37
CF220	5	218.39	349.32	385.29	98.48	49.94	32.48
	15	226.27	372.41	413.94	97.88	49.90	32.00
	25	246.44	389.20	430.25	98.34	49.83	31.68
	35	262.06	402.13	440.42	98.25	48.76	31.51
CF280	5	227.68	348.45	385.75	98.01	61.66	43.40
	15	255.36	373.87	406.97	98.51	61.25	43.60
	25	267.91	387.07	431.20	98.10	62.10	42.06
	35	277.92	398.83	438.48	98.59	61.53	41.65

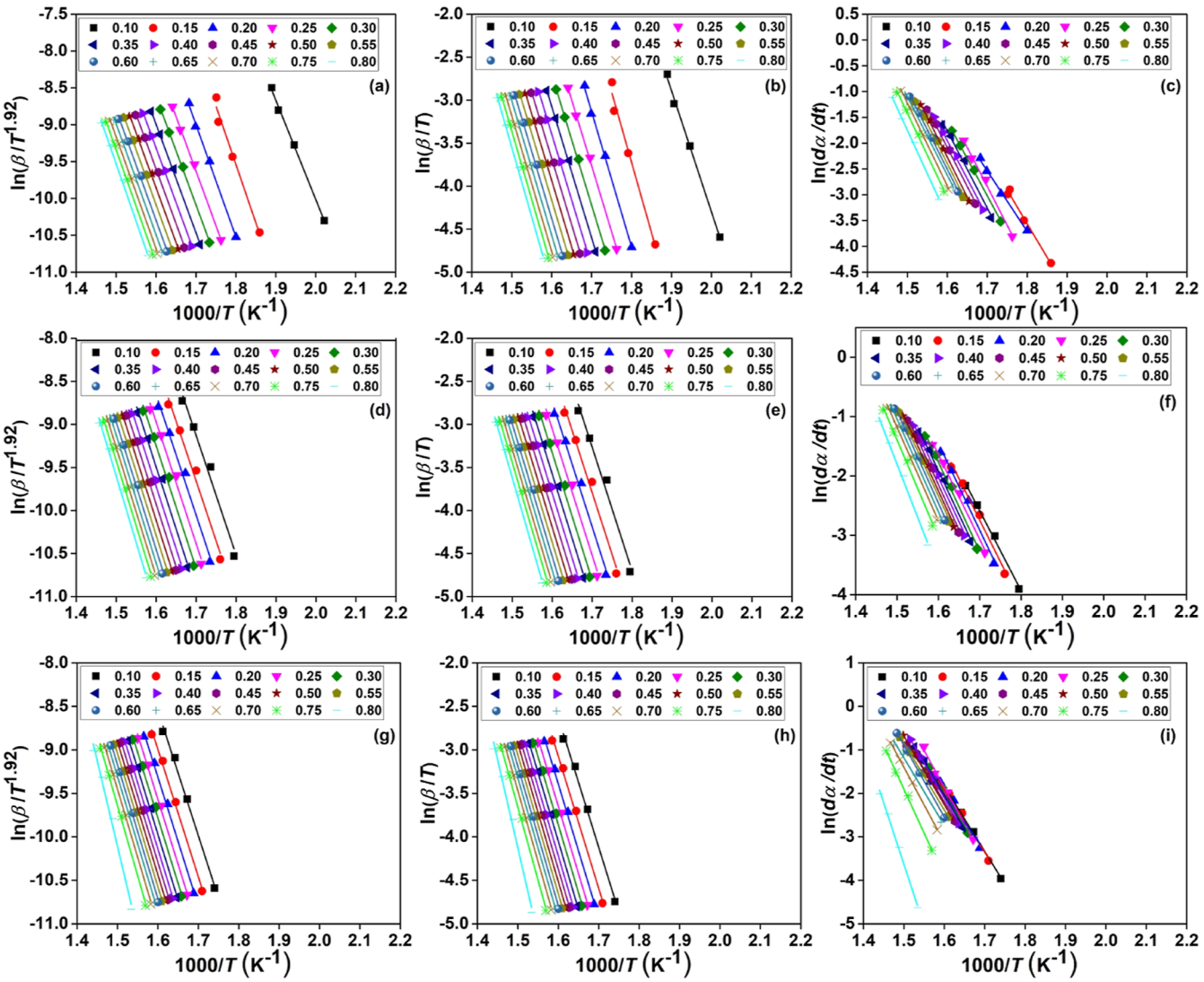

Figure 2. Linear fitted plots for determining the activation energies of (a−c) raw CF, (d−f) CF220, and (g−i) CF280 samples by using Starink (a,d,g), Boswell (b,e,h), and Friedman (c,f,i) methods.

$$\frac{f(\alpha)g(\alpha)}{f(\alpha)_{0.5}g(\alpha)_{0.5}} = \left(\frac{T}{T_{0.5}}\right)^2 \left\{\frac{\left(\frac{d\alpha}{dt}\right)}{\left(\frac{d\alpha}{dt}\right)_{0.5}}\right\} \quad (8)$$

where the subscript 0.5 denotes "at α = 0.5".

Table 1 presents the expressions of various solid-state reaction models and their $g(\alpha)$ and $f(\alpha)$.[20,38,39] By using the $f(\alpha)$ and $g(\alpha)$ of each model, the theoretical curves can be obtained by plotting the left-hand side of eq 8 versus α. Meanwhile, by using the TGA data, the experimental curves are acquired by plotting the right-hand side of eq 8 versus α.

https://doi.org/10.1021/acsomega.3c04328
ACS Omega 2023, 8, 34938−34947

Then, a suitable reaction model could be selected for biomass pyrolysis by comparing the experimental and theoretical curves.

2.5. Thermodynamic Parameters. In this work, the thermodynamic parameters ΔH, ΔG, and ΔS were calculated using the following equations.[40]

$$\Delta H = E_\alpha - RT \tag{9}$$

$$\Delta G = E_\alpha + RT_m \ln\left(\frac{K_B T_m}{hA}\right) \tag{10}$$

$$\Delta S = \frac{\Delta H - \Delta G}{T_m} \tag{11}$$

where K_B and h are the Boltzmann and Planck constants, respectively. Moreover, the T_m and $T(\alpha)$ at the heating rate of 35 °C/min were adopted to obtain these thermodynamic parameters. Note that biomass pyrolysis involves a large number of complex reactions, and these thermodynamic parameters estimated here are only used for providing a supplemental means of understanding the biomass pyrolysis process.

3. RESULTS AND DISCUSSION

3.1. Sample Properties. Table 2 shows the proximate and ultimate analyses, as well as the HHV of raw and torrefied CF samples. With increasing torrefaction severity, the moisture and volatile matter contents decreased, while the fixed carbon and ash contents increased. The torrefaction temperature also influences the ultimate analyses of the samples, and a higher torrefaction temperature leads to higher carbon and lower oxygen contents.[41] Specifically, compared to the raw sample, the carbon content of the CF280 sample rose from 52.38 to 63.25%. The release of moisture and carbon dioxide causes dehydroxylation and decarboxylation reactions, probably resulting in a reduction of oxygen content.[15] Meanwhile, the release of oxygen can also occur in the form of CO and other oxygen-containing gases. Moreover, the hydrogen content seemed to slightly decrease, while the nitrogen content correspondingly increased with increasing the torrefaction temperature. In addition, the HHV increased with the torrefaction temperature, and a high value of 26.13 MJ/kg was observed for the CF280 sample.

3.2. Thermogravimetric Analysis. To investigate the thermal degradation behaviors of raw and torrefied CF samples, pyrolysis experiments were conducted at four different heating rates (i.e., 5, 15, 25, and 35 °C /min). Figure 1 shows the thermogravimetric (TG) and differential thermogravimetric (DTG) curves for pyrolysis of raw CF, CF220, and CF280 samples at different heating rates. As the pyrolysis heating rate increased, the TG and DTG curves shifted to the right, meaning that the temperature at which the major thermal degradation started shifted toward a higher temperature. In general, the pyrolysis process can be roughly classified into three subprocesses, i.e., moisture evaporation (<approximately 130 °C), major thermal degradation (approximately 130−450 °C), and carbonization (>approximately 450 °C).[42] During moisture removal, a small mass loss is observed because the samples have a low moisture content. During the second subprocess, a sharp drop in mass is seen, mostly due to the degradation of hemicellulose and cellulose and also depolymerization of lignin.[43,44] During carbonization, the mass appears to smoothly decline until the final pyrolysis temperature, and the mass loss corresponds to the decomposition of lignin and a few carbonaceous compounds present in tar and char.[45]

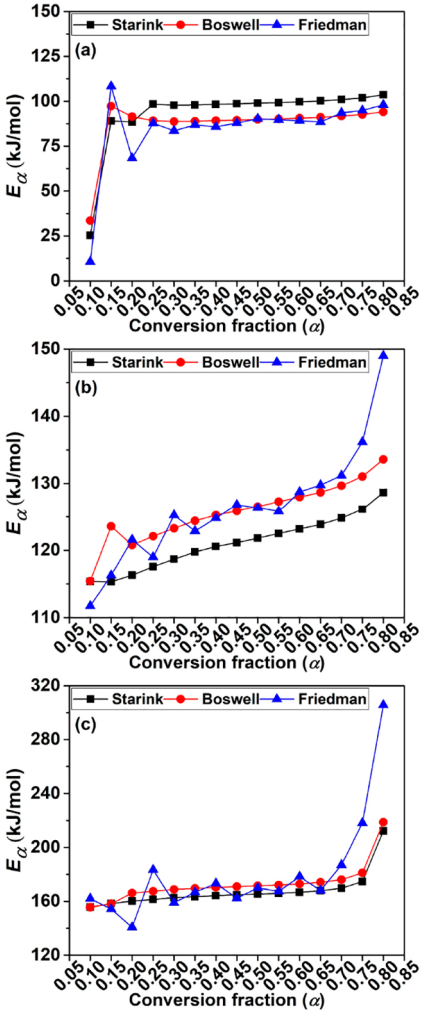

Figure 3. Variation of activation energies with conversion fraction for (a) raw CF, (b) CF220, and (c) CF280 samples by employing the Starink, Boswell, and Friedman methods.

Table 3 presents the temperatures and mass fractions at the start, peak, and end of the major thermal degradation of raw and torrefied CF samples. Specifically, T_a, T_m, and T_c denote the temperatures, while M_a, M_m, and M_c represent the mass fractions at the start, peak, and end of the major thermal degradation, respectively. For each sample, the values of T_a, T_m, and T_c increased with the heating rate. As the torrefaction temperature increased, the value of T_a rose, while the values of T_m and T_c did not change significantly. In general, as the torrefaction severity increases, more volatiles are released during torrefaction; thus, the thermal stability of torrefied samples is enhanced, which leads to a higher T_a.[10,46] In addition, M_a, M_m, and M_c seemed to be nearly independent of the heating rate. After mild torrefaction, the value of M_a increased, but it negligibly varied when the torrefaction temperature was further raised to 280 °C. In contrast, M_m and M_c showed a consistent increase with the torrefaction temperature, although such an increasing trend was more obvious when the torrefaction temperature rose from 220 to 280 °C.

https://doi.org/10.1021/acsomega.3c04328
ACS Omega 2023, 8, 34938−34947

Table 4. Activation Energies, Coefficient of Determination, and Pre-exponential Factors of Raw and Torrefied CF Samples Calculated by Using the Starink, Boswell, and Friedman Methods

species		raw			CF220			CF280		
method	α	E_α (kJ/mol)	R^2	A (s^{-1})	E_α(kJ/mol)	R^2	A (s^{-1})	E_α(kJ/mol)	R^2	A (s^{-1})
Starink	0.10	92.30	0.97540	1.18×10^{7}	115.35	0.97179	8.92×10^{8}	155.65	0.99256	1.83×10^{12}
	0.15	89.03	0.98825	6.34×10^{6}	115.33	0.97937	8.89×10^{8}	158.33	0.99430	3.00×10^{12}
	0.20	88.44	0.99725	5.66×10^{6}	116.30	0.98238	1.07×10^{9}	160.15	0.99450	4.20×10^{12}
	0.25	98.45	0.99872	3.75×10^{7}	117.56	0.98412	1.35×10^{9}	161.36	0.99438	5.25×10^{12}
	0.30	97.81	0.99840	3.32×10^{7}	118.68	0.98542	1.66×10^{9}	162.68	0.99474	6.72×10^{12}
	0.35	97.97	0.99794	3.43×10^{7}	119.74	0.98655	2.03×10^{9}	163.43	0.99471	7.71×10^{12}
	0.40	98.32	0.99753	3.66×10^{7}	120.56	0.98733	2.36×10^{9}	164.12	0.99478	8.77×10^{12}
	0.45	98.59	0.99706	3.85×10^{7}	121.14	0.98779	2.63×10^{9}	164.80	0.99493	9.93×10^{12}
	0.50	98.97	0.99683	4.14×10^{7}	121.80	0.98817	2.97×10^{9}	165.26	0.99502	1.08×10^{13}
	0.55	99.25	0.99652	4.37×10^{7}	122.50	0.98885	3.38×10^{9}	165.85	0.99511	1.21×10^{13}
	0.60	99.71	0.99619	4.75×10^{7}	123.17	0.98914	3.83×10^{9}	166.63	0.99518	1.39×10^{13}
	0.65	100.22	0.99580	5.24×10^{7}	123.84	0.98936	4.35×10^{9}	167.83	0.99528	1.74×10^{13}
	0.70	100.97	0.99571	6.03×10^{7}	124.79	0.98944	5.18×10^{9}	169.67	0.99517	2.45×10^{13}
	0.75	101.93	0.99556	7.22×10^{7}	126.13	0.98954	6.65×10^{9}	174.68	0.99456	6.18×10^{13}
	0.80	103.60	0.99557	9.89×10^{7}	128.65	0.98898	1.06×10^{10}	212.26	0.98436	6.26×10^{16}
average		97.70		4.14×10^{7}	121.04		3.32×10^{9}	167.51		4.19×10^{15}
Boswell	0.10	95.27	0.98686	2.06×10^{7}	115.43	0.97179	9.05×10^{8}	155.53	0.99256	1.78×10^{12}
	0.15	97.32	0.98825	3.03×10^{7}	123.56	0.97937	4.12×10^{9}	158.20	0.99430	2.93×10^{12}
	0.20	91.44	0.99743	9.99×10^{6}	120.79	0.98380	2.46×10^{9}	166.13	0.99496	1.27×10^{13}
	0.25	89.21	0.99882	6.56×10^{6}	122.10	0.98542	3.14×10^{9}	167.40	0.99486	1.61×10^{13}
	0.30	88.71	0.99855	5.96×10^{6}	123.28	0.98661	3.91×10^{9}	168.77	0.99518	2.07×10^{13}
	0.35	88.90	0.99813	6.19×10^{6}	124.38	0.98766	4.81×10^{9}	169.56	0.99516	2.40×10^{13}
	0.40	89.25	0.99775	6.60×10^{6}	125.25	0.98839	5.64×10^{9}	170.30	0.99523	2.75×10^{13}
	0.45	89.52	0.99733	6.95×10^{6}	125.86	0.98881	6.33×10^{9}	171.01	0.99537	3.13×10^{13}
	0.50	89.88	0.99712	7.45×10^{6}	126.56	0.98917	7.20×10^{9}	171.50	0.99545	3.43×10^{13}
	0.55	90.17	0.99683	7.86×10^{6}	127.29	0.98979	8.25×10^{9}	172.13	0.99553	3.85×10^{13}
	0.60	90.59	0.99653	8.51×10^{6}	127.99	0.99006	9.40×10^{9}	172.94	0.99559	4.47×10^{13}
	0.65	91.07	0.99617	9.32×10^{6}	128.69	0.99026	1.07×10^{10}	174.18	0.99569	5.63×10^{13}
	0.70	91.75	0.99609	1.06×10^{7}	129.67	0.99033	1.28×10^{10}	176.05	0.99558	7.95×10^{13}
	0.75	92.61	0.99595	1.25×10^{7}	131.03	0.99042	1.65×10^{10}	181.11	0.99502	2.02×10^{14}
	0.80	94.10	0.99595	1.65×10^{7}	133.59	0.98989	2.66×10^{10}	218.77	0.98537	2.07×10^{17}
average		91.32		1.11×10^{7}	125.70		8.18×10^{9}	172.91		1.38×10^{16}
Friedman	0.10	75.83	0.97747	5.14×10^{5}	111.74	0.99243	4.54×10^{8}	162.00	0.99597	5.92×10^{12}
	0.15	108.34	0.98211	2.40×10^{8}	116.28	0.98494	1.06×10^{9}	154.23	0.97085	1.40×10^{12}
	0.20	68.36	0.99409	1.22×10^{5}	121.58	0.98488	2.85×10^{9}	140.76	0.91593	1.15×10^{11}
	0.25	87.76	0.99340	4.98×10^{6}	118.98	0.98882	1.76×10^{9}	183.37	0.98920	3.07×10^{14}
	0.30	83.57	0.99856	2.25×10^{6}	125.21	0.99042	5.60×10^{9}	158.93	0.98893	3.35×10^{12}
	0.35	86.89	0.98606	4.23×10^{6}	122.86	0.98838	3.62×10^{9}	166.71	0.99532	1.41×10^{13}
	0.40	85.77	0.99634	3.42×10^{6}	124.79	0.99011	5.19×10^{9}	173.24	0.99866	4.73×10^{13}
	0.45	87.91	0.99576	5.12×10^{6}	126.83	0.98744	7.58×10^{9}	162.23	0.97965	6.17×10^{12}
	0.50	90.27	0.99823	8.01×10^{6}	126.34	0.99052	6.92×10^{9}	169.97	0.99562	2.59×10^{13}
	0.55	89.72	0.99221	7.22×10^{6}	125.80	0.99222	6.25×10^{9}	167.38	0.99845	1.60×10^{13}
	0.60	89.19	0.99660	6.53×10^{6}	128.74	0.99023	1.08×10^{10}	178.33	0.99978	1.21×10^{14}
	0.65	88.51	0.99556	5.74×10^{6}	129.76	0.98772	1.31×10^{10}	168.01	0.97977	1.80×10^{13}
	0.70	93.56	0.99692	1.49×10^{7}	131.19	0.99003	1.70×10^{10}	187.03	0.99833	6.03×10^{14}
	0.75	94.86	0.99401	1.91×10^{7}	136.17	0.99222	4.29×10^{10}	218.13	0.99739	1.84×10^{17}
	0.80	98.05	0.99649	3.48×10^{7}	148.99	0.99207	4.61×10^{11}	305.73	0.99312	1.66×10^{24}
average		88.57		2.38×10^{7}	126.35		3.91×10^{10}	179.74		1.11×10^{23}

3.3. Kinetic Parameters. Figure 2 depicts the linear fitted plots for determining the activation energies of raw CF, CF220, and CF280 samples by using the Starink, Boswell, and Friedman methods. For each sample and method, the fitted lines for different α values were mostly parallel to each other, except for some at high α. This indicated that the degradation process broadly obeyed a similar reaction model. Moreover, the lines obtained using the Starink and Boswell methods demonstrated a higher degree of parallelism than those derived from the Friedman method. In addition, the gap between the lines for $0.10 \leq \alpha \leq 0.30$ was larger than that between the lines for $0.40 \leq \alpha \leq 0.70$, and such a difference was more noticeable for the Starink and Boswell methods. This suggested that high energy was required to break down the chemical bonds at the starting stage.[47] Furthermore, the gap between the lines generally decreased after torrefaction, and the lines seemed to be closely packed for the CF280 sample.

https://doi.org/10.1021/acsomega.3c04328
ACS Omega 2023, 8, 34938−34947

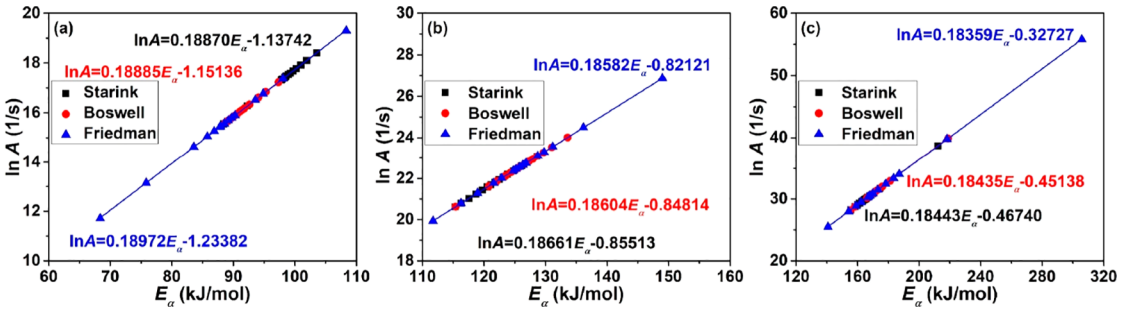

Figure 4. Correlation between the E_α and ln(A) obtained using different methods for (a) raw CF, (b) CF220, and (c) CF280 samples. Note that the black, red, and blue colors represent the fitting equations and lines obtained by the Starink, Boswell, and Friedman methods, respectively.

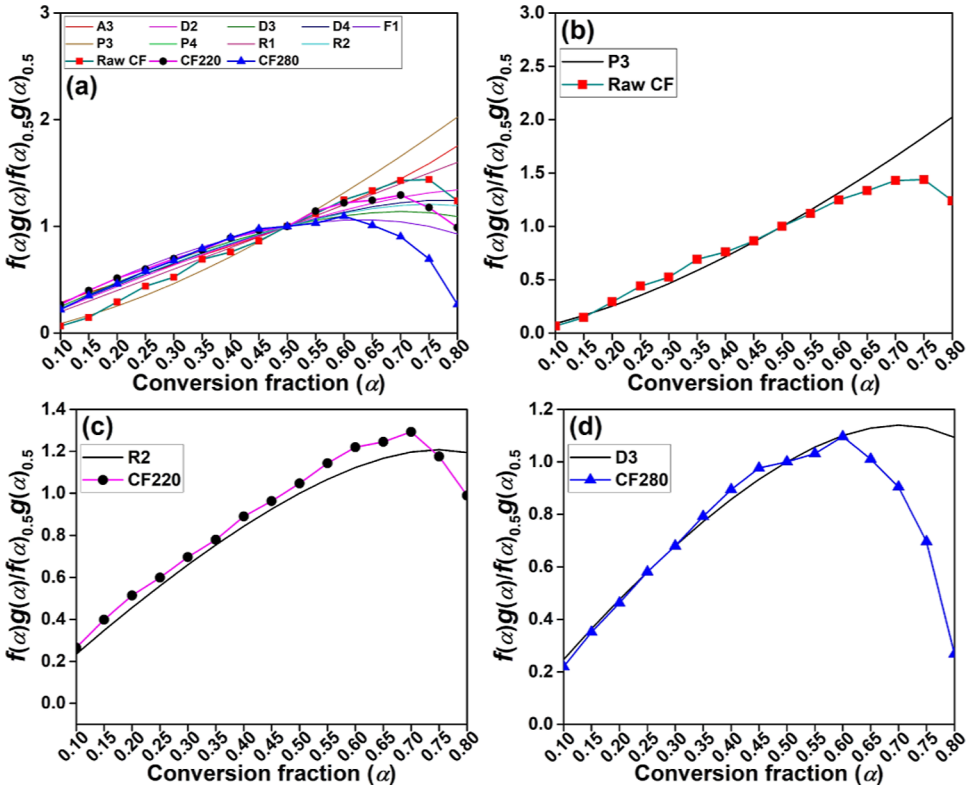

Figure 5. Theoretical and experimental master plots for (a) all three samples, (b) raw CF, (c) CF220, and (d) CF280 samples. The pyrolysis heating rate was 35 °C/min.

Figure 3 shows the variation of E_α with α for raw CF, CF220, and CF280 samples calculated by employing the Starink, Boswell, and Friedman methods. The E_α of all raw and torrefied CF samples generally showed a rising trend as the α increased, although some fluctuations were also observed for the Friedman method. Furthermore, when α ranged from 0.25 to 0.70, the E_α values for raw and CF220 samples estimated by using the Friedman method were quite close to those of the Boswell method. In addition, the E_α values broadly increased with the torrefaction severity, which might be due to the enhanced thermal stability after torrefaction.[31,48]

Table 4 also summarizes the E_α, coefficient of determination (R^2), and A of raw and torrefied CF samples calculated by different methods. For all methods used, high R^2 values ($R^2 > 0.91$) were observed, justifying the accuracy of the kinetic parameters. Through the Starink, Boswell, and Friedman methods, the average E_α for raw CF was 97.70, 91.32, and 88.57 kJ/mol, respectively.

For the CF220 sample, they increased to 121.04, 125.70, and 126.35 kJ/mol, respectively. For the CF280 sample, they further increased to 167.51, 172.91, and 179.74 kJ/mol, respectively. In addition, the A values also increased with torrefaction severity. For the raw CF, the average values of A calculated by using the Starink, Boswell, and Friedman methods were 4.14×10^7, 1.11×10^7, and 2.38×10^7 s^{-1}, respectively. For the CF220 sample, they were 3.32×10^9, 8.18×10^9, and 3.91×10^{10} s^{-1}, respectively. For the CF280 sample, they were 4.19×10^{15}, 1.38×10^{16}, and 1.11×10^{23} s^{-1}, respectively.

3.4. Kinetic Compensation Effect. In general, the kinetic compensation effect (KCE) refers to a phenomenon in which changes in the reaction rate are correspondingly compensated by other governing factors. An increase in the E_α usually decreases the reaction rate. However, the KCE

https://doi.org/10.1021/acsomega.3c04328
ACS Omega 2023, 8, 34938−34947

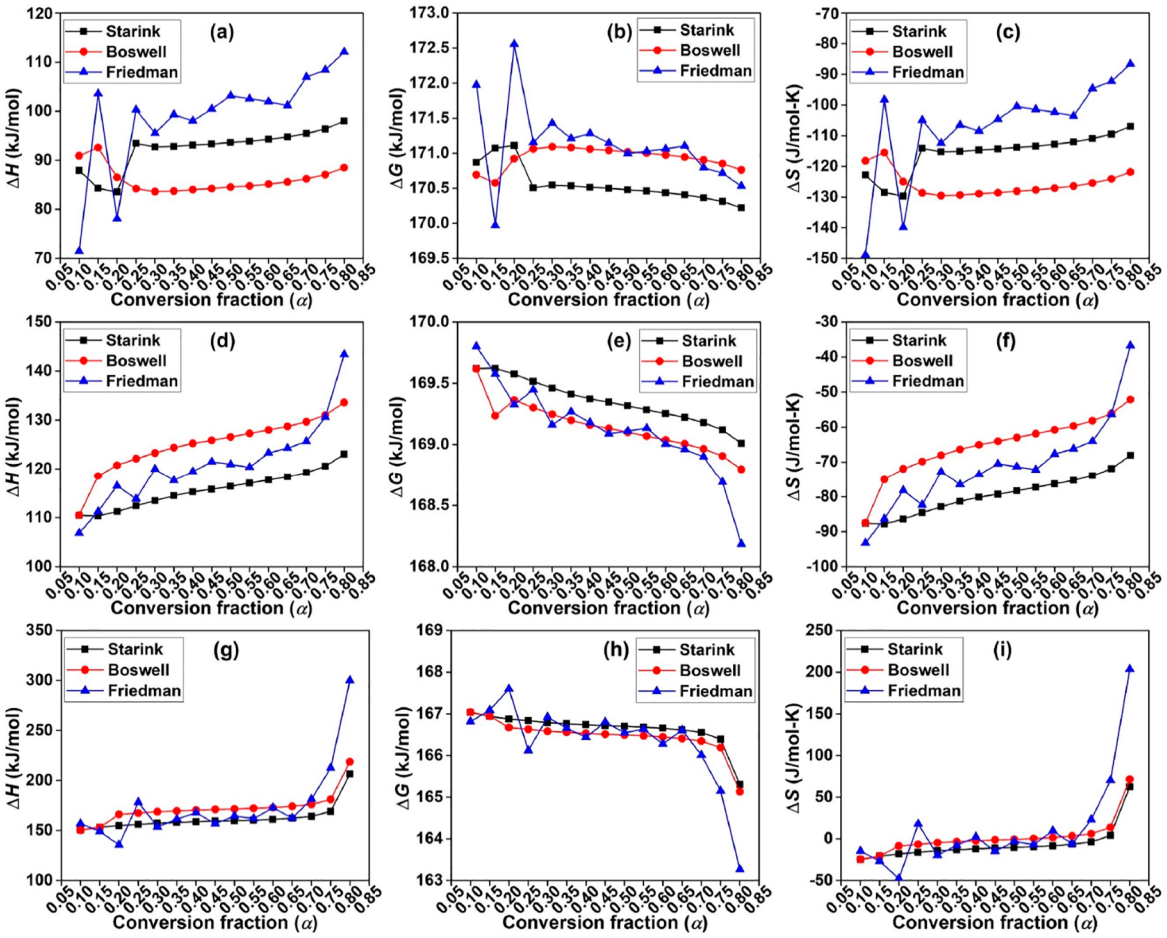

Figure 6. Variation of enthalpy, Gibbs free energy, and entropy with the conversion fraction for (a–c) raw CF, (d–f) CF220, and (g–i) CF280 samples by employing the Starink, Boswell, and Friedman methods.

suggests that other factors such as $\ln(A)$ can show a compensatory change which may lower the effect of increased E_α on the reaction rate. Thus, the KCE highlights the interrelationship between E_α and $\ln(A)$. To explore the KCE during biomass pyrolysis, Figure 4 presents the correlation between the E_α and $\ln(A)$ estimated using different methods for raw CF, CF220, and CF280 samples. Obviously, when $0.10 \leq \alpha \leq 0.80$, a linear relationship between $\ln(A)$ and E_α was observed for all samples and methods, which indicated a compensation effect.

3.5. Determination of the Kinetic Reaction Model. To investigate the reaction mechanism followed by the biomass samples during pyrolysis, the master-plot method was employed. Figure 5 presents the theoretical and experimental master plots for raw CF, CF220, and CF280 samples under the pyrolysis heating rate of 35 °C/min. For the raw CF sample, when $0.1 < \alpha < 0.60$, the experimental curve basically matched the P3 model. Torrefaction severity can influence the reaction mechanism. For the CF220 sample, when $0.1 < \alpha < 0.70$, the experimental curve was generally consistent with the R2 model. For the CF280 sample, when $0.1 < \alpha < 0.60$, the experimental curve was close to the D3 model, showing that the pyrolysis was associated with diffusion reactions. However, at higher α (e.g., $\alpha > 0.7$), the experimental curves failed to match any theoretical model. This was expected because the char formation and the thermal degradation of lignin occurred at a high α.[49]

3.6. Thermodynamic Analysis. Figure 6 depicts the variation of ΔH, ΔG, and ΔS with α for raw CF, CF220, and CF280 samples by employing the Starink, Boswell, and Friedman methods. The ΔH could represent the energy required in converting reactants into an activated complex.[50,51] For the raw CF sample, the Friedman method yielded higher ΔH values than the Starink and Boswell methods within the α range of 0.25–0.80. However, for CF220 and CF280 samples, the ΔH values obtained from the Friedman method were observed to lie in between those of the Starink and Boswell methods within the α ranges of 0.15–0.75 and 0.30–0.65, respectively. In addition, the average ΔH values for raw CF samples using the Starink, Boswell, and Friedman methods were 92.50, 86.11, and 98.87 kJ/mol, respectively. For the CF220 sample, they increased to 115.71, 125.04, and 121.03 kJ/mol, respectively. For the CF280 sample, they further rose to 162.11, 172.22, and 174.33 kJ/mol, respectively. The ΔG provides information about the available amount of energy for the pyrolysis process.[52] For the raw CF and CF220 samples, the ΔG values obtained by using the Friedman method were comparable to those obtained by using the Boswell method within the α ranges of 0.25–0.80 and 0.20–0.70, respectively. Furthermore, the positive values of ΔG indicated a non-spontaneous nature and suggested an external heat input

https://doi.org/10.1021/acsomega.3c04328
ACS Omega 2023, 8, 34938–34947

required for advancing pyrolysis reactions.[53] In addition, when $0.10 \leq \alpha \leq 0.80$ for raw CF and CF220 samples, the ΔS values estimated by using the three methods were negative. In general, the negative ΔS values implied that the disorder decreased. For the CF280 sample, the three methods could produce positive ΔS values for some α. The average ΔS values estimated by using the Starink, Boswell, and Friedman methods were −115.59, −125.61, and −107.02 J/mol·K for the raw CF sample, −79.43, −65.32, and −71.22 J/mol·K for the CF220 sample, and −6.88, 1.54 and 11.91 J/mol·K for the CF280 sample, respectively. Overall, these analyses revealed that the degradation process was endothermic, progressed by forming activated complexes, and necessitated some energy.

4. CONCLUSIONS

In this work, the pyrolysis characteristics and kinetic and thermodynamic analyses of raw and torrefied CF samples were systematically explored. Correspondingly, two distinct torrefaction temperatures (i.e., 220 and 280 °C) and four different pyrolysis heating rates (i.e., 5, 15, 25, and 35 °C/min) were selected. The activation energy for pyrolysis was estimated by adopting three isoconversional methods, i.e., the Starink, Boswell, and Friedman methods. The master-plot method was employed to analyze the reaction mechanism followed by raw and torrefied biomass samples. Furthermore, three thermodynamic parameters, i.e., ΔH, ΔG, and ΔS, were calculated. Results show that the average E_α values of CF220 and CF280 samples were higher than that of the raw CF sample. A compensation effect between the activation energy and pre-exponential factor was observed for all samples. The increased ΔH values indicated a higher energy requirement for torrefied CF samples. The negative values of ΔS implied that the disorder decreased.

AUTHOR INFORMATION

Corresponding Author

Xiaoke Ku − *Department of Engineering Mechanics, Zhejiang University, 310027 Hangzhou, China; State Key Laboratory of Clean Energy Utilization, Zhejiang University, 310027 Hangzhou, China;* orcid.org/0000-0002-2182-3933; Email: xiaokeku@zju.edu.cn

Authors

Yogesh Patil − *Department of Engineering Mechanics, Zhejiang University, 310027 Hangzhou, China*

Vikul Vasudev − *Department of Engineering Mechanics, Zhejiang University, 310027 Hangzhou, China*

Complete contact information is available at: https://pubs.acs.org/10.1021/acsomega.3c04328

Notes

The authors declare no competing financial interest.

ACKNOWLEDGMENTS

This work was financially supported by the Fundamental Research Funds for the Central Universities (project number 2021FZZX001-11), the Zhejiang Provincial Natural Science Foundation of China (project number LXR22A020001), and the National Natural Science Foundation of China (project number 12172328).

REFERENCES

(1) Sharma, A.; Pareek, V.; Zhang, D. Biomass pyrolysis-A review of modelling, process parameters and catalytic studies. *Renewable Sustainable Energy Rev.* **2015**, *50*, 1081−1096.

(2) Park, S.; Kim, S. J.; Oh, K. C.; Cho, L.; Kim, M. J.; Jeong, I. S.; Lee, C. G.; Kim, D. Investigation of agro-byproduct pellet properties and improvement in pellet quality through mixing. *Energy* **2020**, *190*, 116380.

(3) Vasudev, V.; Ku, X.; Lin, J. Combustion Behavior of Algal Biochars Obtained at Different Pyrolysis Heating Rates. *ACS Omega* **2021**, *6*, 19144−19152.

(4) Werner, K.; Pommer, L.; Broström, M. Thermal decomposition of hemicelluloses. *J. Anal. Appl. Pyrolysis* **2014**, *110*, 130−137.

(5) González Martínez, M.; Anca Couce, A.; Dupont, C.; da Silva Perez, D.; Thiéry, S.; Meyer, X. M.; Gourdon, C. Torrefaction of cellulose, hemicelluloses and lignin extracted from woody and agricultural biomass in TGA-GC/MS: Linking production profiles of volatile species to biomass type and macromolecular composition. *Ind. Crops Prod.* **2022**, *176*, 114350.

(6) Chen, L.; Wang, X.; Yang, H.; Lu, Q.; Li, D.; Yang, Q.; Chen, H. Study on pyrolysis behaviors of non-woody lignins with TG-FTIR and Py-GC/MS. *J. Anal. Appl. Pyrolysis* **2015**, *113*, 499−507.

(7) Chen, C.; Qu, B.; Wang, W.; Wang, W.; Ji, G.; Li, A. Rice husk and rice straw torrefaction: Properties and pyrolysis kinetics of raw and torrefied biomass. *Environ. Technol. Innovation* **2021**, *24*, 101872.

(8) Chen, W. H.; Lin, B. J.; Lin, Y. Y.; Chu, Y. S.; Ubando, A. T.; Show, P. L.; Ong, H. C.; Chang, J. S.; Ho, S. H.; Culaba, A. B.; Pétrissans, A.; et al. Progress in biomass torrefaction: Principles, applications and challenges. *Prog. Energy Combust. Sci.* **2021**, *82*, 100887.

(9) Acharya, B.; Sule, I.; Dutta, A. A review on advances of torrefaction technologies for biomass processing. *Biomass Convers. Biorefin.* **2012**, *2*, 349−369.

(10) Cahyanti, M. N.; Doddapaneni, T. R. K. C.; Kikas, T. Biomass torrefaction: An overview on process parameters, economic and environmental aspects and recent advancements. *Bioresour. Technol.* **2020**, *301*, 122737.

(11) Chen, W. H.; Wu, Z. Y.; Chang, J. S. Isothermal and non-isothermal torrefaction characteristics and kinetics of microalga Scenedesmus obliquus CNW-N. *Bioresour. Technol.* **2014**, *155*, 245−251.

(12) González Martínez, M.; Floquet, P.; Dupont, C.; da Silva Perez, D.; Meyer, X. M. Assessing the impact of woody and agricultural biomass variability on its behaviour in torrefaction through Principal Component Analysis. *Biomass Bioenergy* **2020**, *134*, 105474.

(13) Doddapaneni, T. R. K. C.; Konttinen, J.; Hukka, T. I.; Moilanen, A. Influence of torrefaction pretreatment on the pyrolysis of Eucalyptus clone: A study on kinetics, reaction mechanism and heat flow. *Ind. Crops Prod.* **2016**, *92*, 244−254.

(14) Cao, X.; Zhang, J.; Cen, K.; Chen, F.; Chen, D.; Li, Y. Investigation of the relevance between thermal degradation behavior and physicochemical property of cellulose under different torrefaction severities. *Biomass Bioenergy* **2021**, *148*, 106061.

(15) Abu Bakar, M. S.; Ahmed, A.; Jeffery, D. M.; Hidayat, S.; Sukri, R. S.; Mahlia, T. M. I.; Jamil, F.; Khurrum, M. S.; Inayat, A.; Moogi, S.; Park, Y. K. Pyrolysis of solid waste residues from Lemon Myrtle essential oils extraction for bio-oil production. *Bioresour. Technol.* **2020**, *318*, 123913.

(16) Patidar, K.; Singathia, A.; Vashishtha, M.; Kumar Sangal, V.; Upadhyaya, S. Investigation of kinetic and thermodynamic parameters approaches to non-isothermal pyrolysis of mustard stalk using model-free and master plots methods. *Mater. Sci. Energy Technol.* **2022**, *5*, 6−14.

(17) Tabal, A.; Barakat, A.; Aboulkas, A.; El harfi, K. Pyrolysis of ficus nitida wood: Determination of kinetic and thermodynamic parameters. *Fuel* **2021**, *283*, 119253.

(18) Vasudev, V.; Ku, X.; Lin, J. Kinetic study and pyrolysis characteristics of algal and lignocellulosic biomasses. *Bioresour. Technol.* **2019**, *288*, 121496.
(19) Singh, R. K.; Patil, T.; Verma, A.; Tekade, S. P.; Sawarkar, A. N. Insights into kinetics, reaction mechanism, and thermodynamic analysis of pyrolysis of rice straw from rice bowl of India. *Bioresour. Technol. Rep.* **2021**, *13*, 100639.
(20) Ahmad, M. S.; Klemeš, J. J.; Alhumade, H.; Elkamel, A.; Mahmood, A.; Shen, B.; Ibrahim, M.; Mukhtar, A.; Saqib, S.; Asif, S.; Bokhari, A. Thermo-kinetic study to elucidate the bioenergy potential of Maple Leaf Waste (MLW) by pyrolysis, TGA and kinetic modelling. *Fuel* **2021**, *293*, 120349.
(21) Açıkalın, K. Determination of kinetic triplet, thermal degradation behaviour and thermodynamic properties for pyrolysis of a lignocellulosic biomass. *Bioresour. Technol.* **2021**, *337*, 125438.
(22) Sahoo, A.; Kumar, S.; Mohanty, K. Kinetic and thermodynamic analysis of Putranjiva roxburghii (putranjiva) and Cassia fistula (amaltas) non-edible oilseeds using thermogravimetric analyzer. *Renewable Energy* **2021**, *165*, 261−277.
(23) Qi, R.; Xiang, A.; Wang, M.; Jiang, E.; Li, Z.; Xiao, H.; Tan, X. Combustion characteristics and kinetic analysis for pyrolysis char of torrefied pretreament from camellia shell. *Biomass Convers. Biorefin.* **2022**, 1−12.
(24) Huang, H.-H.; Xu, L.-L.; Tong, Z.-K.; Lin, E.-P.; Liu, Q.-P.; Cheng, L.-J.; Zhu, M.-Y. De novo characterization of the Chinese fir (Cunninghamia lanceolata) transcriptome and analysis of candidate genes involved in cellulose and lignin biosynthesis. *BMC Genomics* **2012**, *13*, 648.
(25) Qin, K.; Thunman, H. Diversity of chemical composition and combustion reactivity of various biomass fuels. *Fuel* **2015**, *147*, 161−169.
(26) Friedl, A.; Padouvas, E.; Rotter, H.; Varmuza, K. Prediction of heating values of biomass fuel from elemental composition. *Anal. Chim. Acta* **2005**, *544*, 191−198.
(27) Boswell, P. G. On the calculation of activation energies using a modified Kissinger method. *J. Therm. Anal. Calorim.* **1980**, *18*, 353−358.
(28) Tang, W.; Liu, Y.; Zhang, H.; Wang, C. New approximate formula for Arrhenius temperature integral. *Thermochim. Acta* **2003**, *408*, 39−43.
(29) Yao, Z.; Yu, S.; Su, W.; Wu, W.; Tang, J.; Qi, W. Kinetic studies on the pyrolysis of plastic waste using a combination of model-fitting and model-free methods. *Waste Manage. Res.* **2020**, *38*, 77−85.
(30) Gotor, F. J.; Criado, J. M.; Malek, J.; Koga, N. Kinetic analysis of solid-state reactions: the universality of master plots for analyzing isothermal and nonisothermal experiments. *J. Phys. Chem. A* **2000**, *104*, 10777−10782.
(31) Vyazovkin, S.; Burnham, A. K.; Criado, J. M.; Pérez-Maqueda, L. A.; Popescu, C.; Sbirrazzuoli, N. ICTAC Kinetics Committee recommendations for performing kinetic computations on thermal analysis data. *Thermochim. Acta* **2011**, *520*, 1−19.
(32) He, Q.; Ding, L.; Gong, Y.; Li, W.; Wei, J.; Yu, G. Effect of torrefaction on pinewood pyrolysis kinetics and thermal behavior using thermogravimetric analysis. *Bioresour. Technol.* **2019**, *280*, 104−111.
(33) Starink, M. J. The determination of activation energy from linear heating rate experiments: a comparison of the accuracy of isoconversion methods. *Thermochim. Acta* **2003**, *404*, 163−176.
(34) Ahmad, M. S.; Mehmood, M. A.; Al Ayed, O. S.; Ye, G.; Luo, H.; Ibrahim, M.; Rashid, U.; Arbi Nehdi, I.; Qadir, G. Kinetic analyses and pyrolytic behavior of Para grass (Urochloa mutica) for its bioenergy potential. *Bioresour. Technol.* **2017**, *224*, 708−713.
(35) Kaur, R.; Gera, P.; Jha, M. K.; Bhaskar, T. Pyrolysis kinetics and thermodynamic parameters of castor (Ricinus communis) residue using thermogravimetric analysis. *Bioresour. Technol.* **2018**, *250*, 422−428.
(36) D'Cruz, B.; Samuel, J.; George, L. Characterization, non-isothermal decomposition kinetics and photocatalytic water splitting of green chemically synthesized polyoxoanions of molybdenum containing phosphorus as hetero atom. *Thermochim. Acta* **2014**, *596*, 29−36.
(37) Muigai, H. H.; Choudhury, B. J.; Kalita, P.; Moholkar, V. S. Co−pyrolysis of biomass blends: Characterization, kinetic and thermodynamic analysis. *Biomass Bioenergy* **2020**, *143*, 105839.
(38) Mishra, R. K.; Mohanty, K. Kinetic analysis and pyrolysis behaviour of waste biomass towards its bioenergy potential. *Bioresour. Technol.* **2020**, *311*, 123480.
(39) Yin, F.; Zhuang, Q.; Chang, T.; Zhang, C.; Sun, H.; Sun, Q.; Wang, C.; Li, L. Study on pyrolysis characteristics and kinetics of mixed plastic waste. *J. Mater. Cycles Waste Manage.* **2021**, *23*, 1984−1994.
(40) Mehmood, M. A.; Ye, G.; Luo, H.; Liu, C.; Malik, S.; Afzal, I. L.; Xu, J.; Ahmad, M. S. Pyrolysis and kinetic analyses of Camel grass (Cymbopogon schoenanthus) for bioenergy. *Bioresour. Technol.* **2017**, *228*, 18−24.
(41) Patil, Y.; Ku, X. Comparison and characterization of torrefaction performance and pyrolysis behaviour of softwood and hardwood. *Energy Sources, Part A* **2022**, *44*, 8860−8877.
(42) Chen, G.; Leung, D. Y. C. Experimental investigation of biomass waste, (rice straw, cotton stalk, and pine sawdust), pyrolysis characteristics. *Energy Sources* **2003**, *25*, 331−337.
(43) Mishra, G.; Bhaskar, T. Non isothermal model free kinetics for pyrolysis of rice straw. *Bioresour. Technol.* **2014**, *169*, 614−621.
(44) Sait, H. H.; Hussain, A.; Salema, A. A.; Ani, F. N. Pyrolysis and combustion kinetics of date palm biomass using thermogravimetric analysis. *Bioresour. Technol.* **2012**, *118*, 382−389.
(45) Kumar, A.; Reddy, S. N. Study the catalytic effect on pyrolytic behavior, thermal kinetic and thermodynamic parameters of Ni/Ru/Fe-impregnated sugarcane bagasse via thermogravimetric analysis. *Ind. Crops Prod.* **2022**, *178*, 114564.
(46) da Silva, C. M. S.; Vital, B. R.; Carneiro, A. d. C. O.; Costa, E. V.; de Magalhães, M. A.; Trugilho, P. F. Structural and compositional changes in eucalyptus wood chips subjected to dry torrefaction. *Ind. Crops Prod.* **2017**, *109*, 598−602.
(47) Alves, J. L. F.; Da Silva, J. C. G.; da Silva Filho, V. F.; Alves, R. F.; de Araujo Galdino, W. V.; Andersen, S. L. F.; De Sena, R. F. Determination of the bioenergy potential of Brazilian pine-fruit shell via pyrolysis kinetics, thermodynamic study, and evolved gas analysis. *BioEnergy Res.* **2019**, *12*, 168−183.
(48) Tian, X.; Dai, L.; Wang, Y.; Zeng, Z.; Zhang, S.; Jiang, L.; Yang, X.; Yue, L.; Liu, Y.; Ruan, R. Influence of torrefaction pretreatment on corncobs: A study on fundamental characteristics, thermal behavior, and kinetic. *Bioresour. Technol.* **2020**, *297*, 122490.
(49) Zheng, C.; Li, D.; Ek, M. Mechanism and kinetics of thermal degradation of insulating materials developed from cellulose fiber and fire retardants. *J. Therm. Anal. Calorim.* **2019**, *135*, 3015−3027.
(50) Sriram, A.; Swaminathan, G. Pyrolysis of Musa balbisiana flower petal using thermogravimetric studies. *Bioresour. Technol.* **2018**, *265*, 236−246.
(51) Vasudev, V.; Ku, X.; Lin, J. Pyrolysis of algal biomass: Determination of the kinetic triplet and thermodynamic analysis. *Bioresour. Technol.* **2020**, *317*, 124007.
(52) Maia, A. A. D.; de Morais, L. C. Kinetic parameters of red pepper waste as biomass to solid biofuel. *Bioresour. Technol.* **2016**, *204*, 157−163.
(53) Tao, W.; Zhang, P.; Yang, X.; Li, H.; Liu, Y.; Pan, B. An integrated study on the pyrolysis mecanism of peanut shell based on the kinetic analysis and solid/gas characterization. *Bioresour. Technol.* **2021**, *329*, 124860.

https://doi.org/10.1021/acsomega.3c04328
ACS Omega 2023, 8, 34938−34947